Spectrochimica Acta Part A 90 (2012) 93–108

Contents lists available at SciVerse ScienceDirect

Spectrochimica Acta Part A: Molecular and Biomolecular Spectroscopy

journal homepage: www.elsevier.com/locate/saa

Synthesis, computational, spectroscopic, thermal and antimicrobial activity studies on some metal–urate complexes

Mamdouh S. Masoud[a,*], Alaa E. Ali[b], Medhat A. Shaker[b,c], Gehan S. Elasala[b]

[a] Chemistry Department, Faculty of Science, Alexandria University, Alexandria, Egypt
[b] Chemistry Department, Faculty of Science, Damanhour University, Damanhour, Egypt
[c] Chemistry Department, Faculty of Science, King Abdul-Aziz University, North Jeddah, Saudi Arabia

ARTICLE INFO

Article history:
Received 26 September 2011
Received in revised form 7 January 2012
Accepted 16 January 2012

Keywords:
Uric
Complexes
Synthesis
Spectroscopy
Thermal analysis
Computational

ABSTRACT

New sixteen uric acid metal complexes of different stoichiometry, stereo-chemistries and modes of interactions were synthesized using different metals Cr, Mn, Fe, Co, Ni, Cu, Cd, UO_2, Na and K. The synthesized complexes were characterized by elemental analysis, spectral (IR, UV–Vis and ESR) methods, thermal analysis (TG, DTA and DSC) and magnetic susceptibility studies. Molecular modeling calculations were used to characterize the ligation sites of the free ligand. Furthermore, quantum chemical parameters of uric acid such as the energies of highest occupied molecular orbital (E_{HOMO}), energies of lowest unoccupied molecular orbital (E_{LUMO}), the separation energy ($\Delta E = E_{LUMO} - E_{HOMO}$), the absolute electronegativity, χ, the chemical potential, P_i, the absolute hardness, η and the softness (σ) were obtained for uric acid. Eight different microbial categories were used to study the antimicrobial activity of the free ligand and ten of its complexes. The results indicate that the ligand and its metal complexes possess antimicrobial properties. The stoichiometry of iron–uric acid complex was studied by using different spectrophotometric methods.

1. Introduction

Uric acid (Fig. 1), is the end product of purine metabolism in humans. It exists in human blood plasma at considerably high concentration [1]. It protects unsaturated fatty acids from air oxidation and DNA from damage in systems which generate superoxide and peroxy radicals. It is a naturally occurring antioxidant can serve as a nitrogen source for hydrocarbon degrading bacteria [2]. An abundance of uric acid can be found in pathological mineral deposits such as kidney stones and gouty arthritis in various forms of metal salts [3]. Complexes of uric acid with some metal ions, in particular with Ca^{2+} ions, are known to be formed *in vivo* as gallstones and in the case of articular gout. Some chemical information is available about the interaction of uric acid with bio-metals such as Mg, Ca, Fe, Co, Cu and Zn. Although metal ions participate in many biological processes, however, there is limited data on the synthesis and physical and structural properties of pure metal urate salts. In our group, a series of papers were published to throw light on chemistry of biologically active compounds including nucleic acid bases and their complexes and our research in this direction is continued [4–15]. In the present work, a new series of metal urate complexes were synthesized using different metals of Cr, Mn, Fe, Co, Ni, Cu, Cd, UO_2, Na and K. The free ligand and its complexes were examined systematically in their solid state using physicochemical, computational and biological studies.

2. Experimental

2.1. Synthesis of the investigated complexes

The selected metal salts were dissolved in distilled water while the uric acid ligand was dissolved in an alkaline solution and heated till complete solubility. The complexes were synthesized using different molar M:L ratios (1:1, 1:2, 1:3, 2:3 and 2:1) by adding the ligand solution drop wise with constant stirring to the metal salt, heating the product for 15 min and then cooling. In all cases, the reaction mixture was left overnight and the resulting solid complexes were removed by filtration and then washed several times with water. Finally, the isolated complexes were dried in the oven. The metal contents were determined by atomic absorption and flame photometry techniques as well as usual complexmetric titration procedures [16]. The carbon, hydrogen and nitrogen contents were determined. The halogen content was determined by burning 30 mg of the sample in an oxygen flask in the presence of KOH–H_2O_2 mixture and titrating with a standard $Hg(NO_3)_2$ solution using diphenylcarbazone as an indicator [17]. The analytical data of the

* Corresponding author. Tel.: +2 01223431922; fax: +2 03 3911794.
E-mail address: drmsmasoud@yahoo.com (M.S. Masoud).

1386-1425/$ – see front matter © 2012 Elsevier B.V. All rights reserved.
doi:10.1016/j.saa.2012.01.028

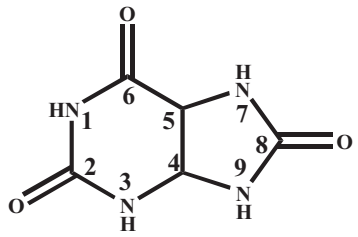

Uric acid, Ua, H_4L

Fig. 1. Uric acid structure.

isolated complexes, Table 1 depict the formation of complexes with different stoichiometries.

2.2. Physical measurements

The KBr disc infrared spectra of the ligands and their complexes were measured over the frequency range 200–4000 cm^{-1} using Perkin-Elmer Spectrophotometer model. Nujol mull electronic spectra were recorded using Perkin-Elmer spectrophotometer model lambda 4B covering the wavelength range 190–900 nm according to the method described by Lee et al. [18]. Molar magnetic susceptibilities, corrected for diamagnetism using Pascal's constants were determined at room temperature (298 °K) using Faraday's method. The instrument was calibrated with $Hg[Co(SCN)_4]$ [19]. The ESR spectra of the copper complexes were recorded at 100 KHz modulation and 10G-modulation amplitude on Varian E-9 spectrometer. The g values were determined by comparison with diphenylbicrylhydrazil radical, DPPH, signal (g = 2.0037) [20]. Differential thermal analysis (DTA), thermogravimetric analysis (TGA) and differential scanning calorimetry (DSC) were carried out using a Shimadzu DTA/TGA-50. The rate of heating was 10 K/min.

2.3. Instrumentation and calculations

The electronic spectra were recorded on a Perkin-Elmer 550 S using 1 cm quartz cells. The molecular structure of free ligand was examined by Chem. 3D Program. The semi empirical calculations were performed with the Hyperchem program Version 5.0.

2.4. Spectrophotometric methods

The molar ratio method [21] permits us to deduce the composition of complexes in solution from spectrophotometry. For this method, solutions containing a constant concentration (4.0×10^{-4} M) of $FeCl_3$ and variable concentration of Ua (from 1.0×10^{-4} to 3.0×10^{-3} M) were prepared at the optimum pH. In order to verify the results of the molar ratio method the complex stoichiometry has also been determined by other methods. For the straight line method [22], two solutions of $FeCl_3$ and Ua with concentrations $[Fe^{3+}]_o$ and $[Ua]_o$, respectively, were placed in a measuring flask of volume, V. To the same volume V_o of the Fe^{3+} component, the volume V of the Ua component is added and the solution was completed to the mark by a supporting electrolyte. The final concentrations of the reagents are: $[Fe^{3+}] = (V_o[Fe^{3+}]_o/V)$ and $[Ua] = (V_o[Ua]_o/V)$. For the continuous variation (Job's method) [23,24], a series of solutions is prepared in which the sum of the total concentration of Ua and Fe(III) is constant, but their proportions are continuously varied. The solutions were obtained by mixing some different volumes of $FeCl_3$ and Ua. The Ua solutions at the same concentration as in the mixture were used for corrections of the Job's plot. For both the slope ratio and limiting logarithmic methods [25], two sets of experiments were constructed. In the first

Table 1
Elemental analysis, m.p, formula, stoichiometries and colour of uric acid (H_4L) complexes. All the complexes have m.p > 300°.

Complexes	Symbol	Color	Calculated/(found) %				
			C	H	N	Metal	Cl
$Cr(H_2L).Cl.3H_2O$	I	Pale-blue	22.09 (22.53)	1.47 (2.11)	20.61 (20.96)	19.14 (18.87)	13.07 (12.81)
$Cr(H_3L)_3.6H_2O$	II	Pale-blue	27.21 (27.64)	3.17 (3.42)	25.40 (25.82)	7.86 (7.91)	–
$Mn(H_2L).2H_2O$	III	Beige	23.34 (23.71)	2.33 (2.64)	21.79 (22.33)	21.37 (21.74)	–
$Fe_2L.2OH.4H_2O$	IV	Brown	16.54 (17.11)	1.93 (2.45)	15.44 (16.12)	30.78 (30.25)	–
$Co(H_2L).2H_2O$	V	Violet	22.98 (22.15)	2.30 (2.35)	21.45 (22.12)	22.58 (22.32)	–
$Co(H_3L)_2.2H_2O$	VI	Violet	27.96 (28.13)	2.33 (2.42)	26.09 (26.90)	13.73 (14.1)	–
$Co_2(H_2L)_2H_4L.6H_2O$	VII	Pale-pink	24.79 (25.63)	2.75 (2.94)	23.13 (23.45)	16.23 (16.35)	–
$Ni(H_3L).Cl.3H_2O$	VIII	Pale-green	18.97 (19.33)	2.85 (3.12)	17.70 (18.14)	18.56 (18.11)	11.22 (11.75)
$Ni(H_4L)_2.Cl_2.2H_2O$	IX	Pale-green	23.91 (24.45)	2.39 (2.55)	22.31 (22.71)	11.70 (12.04)	14.15 (13.76)
$Cu(H_3L)_2H_4L.6H_2O$	X	Yellowish green	26.71 (27.11)	3.26 (3.45)	24.93 (25.11)	9.43 (9.42)	–
$Cu(H_3L)_2.H_2O$	XI	Pale-green	28.86 (29.32)	1.92 (2.33)	26.93 (27.12)	15.28 (15.71)	–
$Cu_2.L.4H_2O$	XII	Dark green	16.56 (17.31)	1.93 (2.12)	15.46 (16.10)	35.08 (34.91)	–
$Cd(H_2L).2H_2O$	XIII	White	19.08 (19.67)	1.91 (2.23)	17.80 (18.22)	35.74 (36.22)	–
$UO_2(H_3L)_2.4H_2O$	XIV	Yellow	17.74 (18.31)	2.07 (2.51)	16.56 (17.08)	35.19 (35.55)	–
$Na_2(H_2L).2H_2O$	XV	White	24.18 (24.95)	2.42 (2.86)	22.57 (23.11)	18.54 (18.11)	–
$K(H_3L).6H_2O$	XVI	White	19.09 (19.66)	4.77 (5.12)	17.82 (18.11)	12.44 (11.98)	–

set, the concentration of the ligand was kept constant and in excess at 2.0×10^{-3} M, while that of $FeCl_3$ was varied from 1.0×10^{-4} to 6.0×10^{-4} M. In the other set, the concentration of $FeCl_3$ was kept constant and in excess at 2.0×10^{-3} M, while the concentration of the Ua was varied from 1.0×10^{-4} to 6.0×10^{-4} M. The successive method was constructed depending on the changes of both the concentrations of the ligand and the metal ion.

2.5. Computational study

The molecular structure of free ligand was examined by Chem. 3D Program as well as hyperchemistry program. The molecule was built with the GaussView 3.0 implemented in Gaussian 03 package.

3. Results and discussions

3.1. Molecular modeling

Generally, the molecular modeling calculations are widely increasing nowadays for the expectation of the mechanism of the reactions and the identification of the products [26]. This saves time and money. The multidentate ligands including nitrogen and oxygen atoms are versatile and useful for assembly new molecules, because they can coordinate many transition metal ions. Thus the synthesis and structures of new complexes are significant for understanding the biological phenomena and exploiting artificial models [27]. Also, a theoretical support for the experimental findings regarding the donor atoms could be obtained on comparing the molecular models of the complexes with that of the free ligands. Geometrical structure and electronic properties of the free ligand, Ua were calculated by optimizing its bond lengths, bond angles and dihedral angles, collected in Table 2 and shown in Fig. 2. The calculations are based on neglecting the possibility of hydrogen bonding. Molecular modeling is a collective term that refers to theoretical methods and computational techniques to model the behaviors of molecules [28,29]. Uric acid coordinates to different metal ions through the protonated N-7 within the imidazole ring and O-14 within the pyrimidine ring. These two atoms carry more electronegative charge confirming active sites for coordination, Table 1. The charge values for N-7 and O-14 are −0.166 and −0.346, respectively. For Ua, the bond lengths are around 1.4 Å. This value decreases for C(1)–O(13) = 1.223, C(3)–O(14) = 1.218, C(8)–O(10) = 1.218, N(2)–H(12) = 0.999, N(6)–H(11) = 0.995, N(7)–H(16) = 0.992 and N(9)–H(15) = 0.992. It is obvious that all C–N bond lengths > C–O bond lengths. As the electronegativity increases, the bond length decreases [30]. On considering the bond angles of Ua, they were found around 120° and 109.5°. These angles are due to sp^2 and sp^3 hybridization of the atoms. The big deviations appear in the region where the two rings, six membered pyrimidine and five membered imidazole rings, are fused together C(3)–C(4)–N(7) = 129.78°, N(6)–C(5)–N(9) = 129.14°. The dihedral angles proved the near planarity of the Ua molecule, where the angles were of nearly 180° and 0°. The difference is due to the *syn* and *anti* positions of the investigated atoms, where the anti gives 180° and the syn gives 0°.

3.1.1. Theoretical study using hyperchemistry

Quantum chemical parameters of organic compounds are obtained from calculations such as energies of the highest occupied molecular orbital, E_{HOMO}, energies of the lowest unoccupied molecular orbital, E_{LUMO}, separation energies, ΔE, absolute electronegativities, χ, chemical potentials, P_i, absolute hardness, η, and absolute softness, σ according to the following equations [31,32]:

$$\Delta E = E_{LUMO} - E_{HOMO}$$

$$\chi = \frac{-(E_{HOMO} + E_{LUMO})}{2}$$

$$\eta = \frac{E_{LUMO} - E_{HOMO}}{2}$$

$$\sigma = \frac{1}{\eta} \quad P_i = -\chi$$

E_{HOMO} is a quantum chemical descriptor which is often associated with the electron donating ability of the molecule. The energy of the lowest unoccupied molecular orbital, E_{LUMO}, indicates the ability of the molecule to accept electrons. The concepts of the parameters, χ and P_i are related to each other. The inverse of the global hardness is designated as the softness, σ [33]. All these quantum chemical parameters were calculated for Ua (Table 3). According to the frontier molecular orbital theory, FMO, the chemical reactivity is a function of interaction between HOMO and LUMO levels of the reacting species [34]. The E_{HOMO} indicates the ability of the molecule to donate electrons to an appropriate acceptor such as metal ions with empty molecular orbitals and E_{LUMO} indicates its ability to accept electrons. The higher is the value of E_{HOMO} of Ua, the easer is its offering electrons to the unoccupied d-orbital of metal ion. The calculations showed that the high energy E_{HOMO} is assigned for the Ua, which is expected to have a good coordination tendency to metal ions. Ua coordinates to different metal ions through the protonated N-7 within the imidazole ring and O-14 within the pyrimidine ring. These two atoms carry more electronegative charge confirming active sites for coordination. Furthermore, the HOMO level is mostly localized on the protonated N-7 within the imidazole ring and O-14 within the pyrimidine ring indicating their being the preferred sites for nucleophilic attack at the central metal ions (Fig. 2). This means that these moieties with high coefficients of HOMO density were oriented toward the metal ions. The HOMO–LUMO energy gap, ΔE approach, which is an important stability index, is applied to develop theoretical model for explaining the structure and conformation barriers in many molecular systems. The high value of ΔE could be expected to indicate Ua molecule has high inclination to bind to the metal ion. Absolute hardness, η and softness, σ are important properties to measure the molecular stability and reactivity. A hard molecule has a large energy gap and a soft molecule has a small energy gap. Soft molecules are more reactive than hard ones because they could easily offer electrons to an acceptor. In a complex formation system, the ligand acts as a Lewis base while the metal ion acts as a Lewis acid. Metal ions are soft acids and thus soft base ligands are most effective for complex formation. Accordingly, it is concluded that Ua with a proper value σ value has a good tendency to chelate metal ions effectively. This is also confirmed from the calculated chemical potential, P_i.

3.2. IR spectra of Ua and its complexes

The fundamental IR bands of Ua and its metal complexes are given in Tables 4 and 5. The free ligand has major peaks at 3013 and 2871 cm^{-1} in weak appearance assigned to N–H stretching. However, strong band at 1680 cm^{-1} is assigned to C=O group. The bands at 1122, 1434, 878 and 785 cm^{-1} were assigned to $\nu_{C-O,}$ $\nu_{C=N,}$ $\delta_{OH,}$ $\delta_{NH,}$ respectively. On the other hand, the ν_{C-N}, $\delta_{(C=O)}$ bands at 1326 and 704 cm^{-1} are strong evidence that the structure of the ligand is keto–enol tautomerized before complexation with metal ions [35]. Three oxygen and four NH bonds are available for hydrogen bonding formation and thus Ua can be considered as a good electron donor [36]. The examination of the IR spectra of its metal complexes shows broad bands in the region of 3450–3510 cm^{-1} for the complexes I, III, IV, V, VI, VII, VIII, XII and XIII, which suggests

Table 2
Molecular modeling data of uric acid (H_4L^1).

Charge density			
Atoms	Actual	Atoms	Actual
C(1)	0.208	N(9)	−0.107
N(2)	−0.009	O(10)	−0.350
C(3)	0.345	H(11)	0.096
C(4)	0.335	H(12)	0.123
C(5)	−0.148	O(13)	−0.372
N(6)	−0.139	O(14)	−0.346
N(7)	−0.166	H(15)	0.098
C(8)	0.176	H(16)	0.101
Bond length (A°)			
C(1)–N(2)	1.414	N(6)–C(1)	1.439
C(1)–O(13)	1.223	C(4)–N(7)	1.435
N(2)–C(3)	1.437	N(7)–H(16)	0.992
N(2)–H(12)	0.999	N(7)–C(8)	1.438
C(3)–O(14)	1.218	C(8)–O(10)	1.218
C(3)–C(4)	1.455	C(8)–N(9)	1.457
C(4)–C(5)	1.379	N(9)–H(15)	0.992
C(5)–N(6)	1.409	N(9)–C(5)	1.425
N(6)–H(11)	0.995		
Bond angle			
O(13)–C(1)–N(2)	118.648	C(5)–C(4)–N(7)	109.612
O(13)–C(1)–N(6)	118.648	C(3)–C(4)–N(7)	129.778
N(2)–C(1)–N(6)	122.705	C(4)–C(5)–N(9)	109.106
C(1)–N(2)–C(3)	121.143	N(6)–C(5)–N(9)	129.142
C(1)–N(2)–H(12)	119.429	C(4)–N(7)–H(16)	127.132
C(3)–N(2)–H(12)	119.429	C(4)–N(7)–C(8)	105.736
N(2)–C(3)–O(14)	122.346	H(16)–N(7)–C(8)	127.132
N(2)–C(3)–C(4)	115.308	N(7)–C(8)–O(10)	125.22
O(14)–C(3)–C(4)	122.346	N(7)–C(8)–N(9)	109.56
C(3)–C(4)–C(5)	120.611	N(9)–C(8)–O(10)	125.22
C(4)–C(5)–N(6)	121.752	C(8)–N(9)–H(15)	127.007
C(5)–N(6)–C(1)	118.482	C(8)–N(9)–C(5)	105.986
C(5)–N(6)–H(11)	120.759	C(5)–N(9)–H(15)	127.007
C(1)–N(6)–H(11)	120.759		
Dihedral angle			
O(13)–C(1)–N(6)–H(11)	−0.0351	C(3)–C(4)–C(5)–N(9)	179.98
N(2)–C(1)–N(6)–C(5)	0.0351	N(7)–C(4)–C(5)–N(6)	180
N(2)–C(1)–N(6)–H(11)	180	N(6)–C(5)–N(9)–H(15)	0.0517
O(13)–C(1)–N(6)–C(5)	180	C(4)–C(5)–N(9)–C(8)	1.5843
O(13)–C(1)–N(2)–H(12)	−0.0834	C(4)–C(5)–N(9)–H(15)	180
N(6)–C(1)–N(2)–C(3)	−0.1282	N(6)–C(5)–N(9)–C(9)	−179.934
O(13)–C(1)–N(2)–C(3)	179.917	C(5)–N(9)–C(8)–N(7)	−0.0679
N(6)–C(1)–N(2)–H(12)	179.872	H(15)–N(9)–C(8)–O(10)	1.5843
H(12)–N(2)–C(3)–O(14)	0.100018	C(5)–N(9)–C(8)–O(10)	180
C(1)–N(2)–C(3)–C(4)	0.100018	H(15)–N(9)–C(8)–N(7)	179.946
H(12)–N(2)–C(3)–C(4)	−179.9	N(9)–C(8)–N(7)–C(4)	0.100098
C(1)–N(2)–C(3)–O(14)	−179.9	O(10)–C(8)–N(7)–H(16)	−0.0679
O(14)–C(3)–C(4)–N(7)	−0.10083	N(9)–C(8)–N(7)–H(16)	180
N(2)–C(3)–C(4)–C(5)	0	O(10)–C(8)–N(7)–C(4)	−179.983
N(2)–C(3)–C(4)–N(7)	179.899	H(16)–N(7)–C(4)–C(3)	0.100098
O(14)–C(3)–C(4)–C(5)	180	C(8)–N(7)–C(4)–C(5)	−0.09153
C(3)–C(4)–C(5)–N(6)	−0.0809	C(8)–N(7)–C(4)–C(3)	180
N(7)–C(4)–C(5)–N(9)	0.04596	H(16)–N(7)–C(4)–C(5)	180

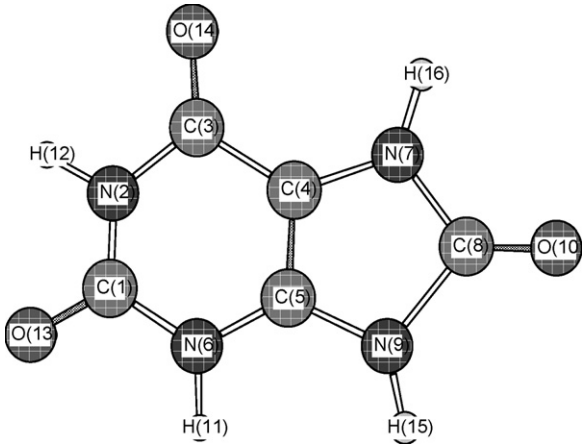

Fig. 2. The Molecular modeling of uric acid.

Table 3
The calculated quantum chemical parameters of uric acid.

Parameter	Calculated value
HOMO (eV)	−8.853
LUMO (eV)	−0.730
ΔE (eV)	8.123
χ (electronegativity)	4.792
P_i (chemical potential)	−4.792
η (hardness)	4.062
σ (softness)	0.246

the coordination with water. Meanwhile, the bands in the region of 3300–3500 cm^{-1} for the complexes II, IX, X, XI, XIV, XV and XVI could be taken as an indication of lattice water. It seems from the elemental and thermal analyses of these complexes that they contain water molecules in their structures, which is confirmed by the presence of ν_{OH} and metal–oxygen bands attributed to rocking modes in the region of 503–534 cm^{-1} [37]. For all complexes, the $\nu_{C=O}$ bands are shifted to lower wave number since the resonance increases the single bond character and thus these bands become weaker and are blue shifted or disappeared (complex IV). Also, the band of $\delta_{C=O}$ is shifted to lower wave numbers in all complexes compared to that of Ua, indicating that at least one of the three carbonyl groups in Ua is coordinated to the metal ions. Other characteristic feature of Ua complexes is that the doublet ν_{NH} bands of the free ligand at 3013 and 2871 cm^{-1} are strongly affected on complexation with the presence of only one band in the range 2950–3192 cm^{-1} with different shapes [38]. So the NH groups either participate in bond formation with the metal ions or tautomerized with the adjacent groups to form the keto–enol tautomers [35]. Also, the band at about 785 cm^{-1} for Ua is affected on complexation and δ_{N-H} is shifted to lower wave number in all complexes. In general, one can say that the N–H group is mandatory site for the metal–ligand binding. All Ua complexes gave new well characterized bands due to ν_{M-O} and ν_{M-N} stretching vibrations at 496–534 cm^{-1} and 492–440 cm^{-1}, respectively. For the complexes I, VIII and IX, another characteristic band due to M–Cl in 320–352 cm^{-1} region appears. These new bands are not present in the free ligand [39,40]. The appearance of $\nu_{C=N}$, ν_{C-N}, ν_{N-H}, $\nu_{C=O}$, $\delta_{C=O}$, δ_{OH} and δ_{N-H} in Ua and its complexes with different degrees is strongly evident that the ligand is tautomerized [35]. Ua can form chelate ring system because it has more than one point of attachment to the metal. This chelate system contains five membered rings [38] that give high stability to the newly formed complexes. So, Ua acts as a bidentate ligand through one coordinating group C=O and one acidic group NH, also it acts as a tetradentate in case of the complex XII and a hexadentate ligand in case of the complex IV. Ua can bind to the alkali metals such as Na^+ and K^+ in different ratios (2:1 and 1:1), respectively [41]. This is because Na^+ has small size than K^+ and the charge density on Na^+ is higher than K^+. So, in case of Na^+ the most stable complex is with the ratio 2:1 but in case of K^+ the most stable complex is with the ratio 1:1. Furthermore, Na^+ is considered harder than K^+. Therefore, there are stronger interactions between nitrogen or oxygen and Na^+ than those of nitrogen or oxygen and K^+ according to the hard and soft acid base principle (HSAB) which states that a hard acid prefers to

Table 4
Fundamental infrared bands (cm^{-1}) of uric acid and its complexes (I–VII).

Uric acid	I	II	III	IV	V	VI	VII	Assignments
–	3350(b)	3457(b)	3510(w)	3500(w)	3455(b)	3450(b)	3450(b)	ν_{O-H} of H_2O
3013(w)	3015(m)	3010(w)	3078(m)	3011(m)	3192(w)	3158(m)	3120(w)	ν_{N-H}
2871(w)								
1680(vs)	1670(m)	1666(vs)	–	1679(vs)	1613(m)	1674(m)	1675(s)	$\nu_{C=O}$
	–	–		–	–	1545(w)	–	
1587(vs)	1556(w)	1529(w)	–	1587(w)	1535(m)	1532(w)	1600(m)	$\nu_{C=C}$
1434(w)	1430(m)	1454(m)	1407(m)	1404(m)	1405(w)	1440(m)	1460(w)	$\nu_{C=N}$
1368(m)	1390(s)	1384(s)	1340(w)	1349(w)	1375(s)	1390(s)	1383(m)	ν_{C-C}
1122(vs)	1105(w)	1120(w)	1135(s)	1119(s)	1126(s)	1005(s)	1138(m)	ν_{C-O}
1326(m)	1260(m)	1275(m)	1290(m)	1306(m)	1225(w)	1290(m)	1250(w)	ν_{C-N}
878(m)	871(m)	880(m)	852(m)	870(W)	880(W)	872(m)	–	δ_{OH}
785(s)	767(s)	755(m)	770(m)	784(s)	783(S)	782(m)	784(m)	$\delta_{(N-H)}$
704(s)	682(w)	680(m)	643(w)	680(w)	613(w)	683(m)	679(w)	$\delta_{(C=O)}$
–	507(s)	506(m)	534(s)	504(w)	504(m)	508(s)	506(w)	υ_{M-O}
–	492(m)	492(w)	434(m)	490(m)	485(w)	492(m)	492(w)	υ_{M-N}
	–	320(w)	–	–	–	–	–	υ_{M-Cl}

Abbreviations: vs (very strong), s (strong), m (medium), w (weak).

Table 5
Fundamental infrared bands (cm^{-1}) of uric acid-complexes (VIII–XVI).

VIII	IX	X	XI	XII	XIII	XIV	XV	XVI	Assignments
3451(b)	3350(w)	3350(b)	3350(w)	3450(b)	3450(b)	3350(m)	3300(b)	3320(m)	ν_{O-H} of H_2O
3015(w)	3050(w)	3135(w)	3137(m)	2950(w)	3184(w)	3011(w)	3040(m)	3010(w)	ν_{N-H}
1662(vs)	1664(vs)	1659(s)	1674(s)	1628(vs)	1691(s)	1674(vs)	1660(vs)	1668(vs)	$\nu_{C=O}$
		1545(m)	1590(w)						
1525(w)	1535(m)	1527(m)	1487(w)	1520(w)	1596(m)	1520 (m)	1529(m)	1533(w)	$\nu_{C=C}$ & $\nu_{C=N}$
1420(w)	1450(m)	1429(m)	1436(w)	1463(w)	1417(m)	1432(w)	1429(w)	1437(m)	
1380(s)	1385(s)	1384(s)	1350(w)	1383(s)	1371(s)	1342(w)	1382(m)	1387(s)	ν_{C-C}
1050(m)	1124(m)	1137(s)	1115(m)	1113(m)	1124(s)	1123(m)	1005(m)	1010(w)	ν_{C-O}
1280(w)	1285(m)	1278(m)	–	1222(w)	1280 (w)	1310 (w)	1257(m)	1262(m)	ν_{C-N}
847(m)	871(w)	871(w)	878(m)	837(m)	832(w)	878(w)	880(w)	850(w)	δ_{OH}
753(m)	783(m)	784(s)	784(m)	766(m)	768(m)	785(m)	783 (m)	786(s)	$\delta_{(N-H)}$
704(w)	690 (w)	695(m)	706(m)	708(w)	711(s)	707(w)	620(w)	695(w)	$\delta_{(C=O)}$
503(w)	506(m)	503(m)	509(w)	514(w)	515(m)	501(m)	496	499(w)	υ_{M-O}
491(s)	492(m)	491(w)	485(w)	480(w)	470(w)	440(w)	470(w)	440(w)	υ_{M-N}
350(w)	352(w)	–	–	–	–	–	–	–	υ_{M-Cl}

Abbreviations: vs (very strong), s (strong), m (medium), w (weak).

Table 6
Coordination bond length r (Å) of some uric acid complexes.

Complex	r_{M-N} (Å)	r_{M-O} (Å)
V	0.463	0.865
VI	0.633	0.866
VII	0.423	0.447
VIII	0.477	0.650
IX	0.496	0.653
X	0.601	0.597
XI	1.210	0.810
XII	0.453	0.473

react with a hard base and a soft acid prefers to react with a soft base [42]. The IR spectrum of the complex XIV displays two bands at 908 and 800 cm^{-1}, assigned to υ_3 and υ_1 vibrations of the dioxouranium ion, respectively [43]. The υ_3 value is used to calculate the force constant (F) of $\nu_{U=O}$ by the method of McGlynn et al. [43].

$$(\upsilon_3)^2 = \frac{(1307)^2(F_{U-O})}{14.103}$$

The force constant obtained for uranyl complex was then substituted into the following relation to give an estimate of the U–O bond length in Å [44]. The calculated F_{U-O} and R_{U-O} (U–O bond length) values are 6.81 mdynes $Å^{-1}$ and 1.74 Å, respectively which fall in the usual range of the uranyl complexes

$$R_{U-O} = 1.08(F_{U-O})^{-1/3} + 1.17$$

3.2.1. Calculation of the coordination bond length

The calculations are based on recording the change in the frequency of the band positions of the free ligand with respect to its complexes. If the C=N or C=O groups obtained by tautomerism are suggested to bind to the metal ion, the coordination bond length (r) can be determined from the following equation [45–47].

$$\Delta\upsilon = \left(\frac{32\pi\alpha}{\alpha^2}\right)\left(\frac{\upsilon_{x=y} - \upsilon_{x-y}}{\ell}\right)\exp\left(-2\pi\sqrt{\frac{2r}{a}}\right)$$

$\Delta\upsilon$ is the shift in the oscillator frequency ($\Delta\upsilon = \upsilon_{ligand} - \upsilon_{complex}$) and α is the bond polarizability. The α values were computed based on published data for complexes of similar structures to the present complexes, which are 48.61, 46.59 and 42.50 for cobalt, nickel and copper, respectively [46]. The lattice constant, *a,* of the metal salt are 3.5, 3.524 and 3.614 for cobalt, nickel and copper, respectively [47]. The frequency of the oscillator with a double bond, $\upsilon_{x=y}$ are υ(C=N) and υ(C=O), respectively. The frequency of the oscillator with a single bond, $\upsilon_{x=y}$ are υ(C–N) and υ(C–O), respectively. ℓ is the length of the oscillator coordinated to the metal ion. From such data, the r-values for the bond between the metal and the nitrogen atom of the C=N group and the oxygen atom of the C=O group are computed [48] and collected in Table 6. For these complexes, the values of the calculated coordination bond length of the transition metal complexes decrease in the sequence either to the oxygen or the nitrogen atom: Ni < Co < Cu. For the tetrahedral complex XI, the coordination bond length is longer than that of the octahedral Co(II) and Ni(II) complexes. Thus, the geometry of the complex compound plays a major factor for controlling such trends. In general, the M–O bond length is greater than that of M–N but the reverse case is observed in case of the complexes X and XI.

3.3. Electronic spectral and magnetic studies

Nujol mull electronic absorption spectral data (λ_{max}, nm), room temperature effective magnetic moment values (μ_{eff}, 298 °K) and geometries of the investigated complexes are given in Table 7. The nujol mull electronic absorption spectra for the pale-blue complexes I and II showed three bands at 250, 300 and 510 nm and 310, 425 and 580 nm, respectively due to $^4A_{2g} \rightarrow {}^4T_{2g}$ (F), $^4A_{2g} \rightarrow {}^4T_{1g}$(F) and $^4A_{2g} \rightarrow {}^4T_{1g}$(P) transitions, respectively. So that, these two complexes have octahedral geometries in high spin state [49]. Such O_h geometry is further deduced from the μ_{eff} values, which equals 3.85 and 3.87 B.M, respectively. The beige complex III has the room temperature μ_{eff} value of 5.77 B.M typifying the existence of T_d configuration in high spin state. The electronic spectra of the black complex IV gave bands at 300, 340, 475 and 635 nm and 230, 305, 372 and 500 nm. These bands are due to CT ($t_{2g} \rightarrow \pi^*$) and CT ($\pi \rightarrow e_g$), respectively. Its room temperature μ_{eff} value is 5.91 B.M, typifying the existence of O_h configuration in high spin state. The nujol mull electronic absorption spectra of the complex V gave bands at 235, 310 and 450 nm. The latter broad band is assigned to $^4A_2 \rightarrow {}^4T_1$(P) transition indicating the tetrahedral structure [50]. The μ_{eff} magnetic moment value 4.92 B.M verified such geometry. However, the electronic spectra of complexes VI and VII (Table 7) gave bands in the range of 251–600 nm. The first band is of charge transfer nature and the latter broad band is assigned to $^4T_{1g}$(F) $\rightarrow {}^4T_{1g}$(P) transition. Their magnetic moment values are 5.12 and 5.31, respectively typifying O_h geometry [51]. The nujol mull electronic spectra of the nickel complexes VIII and IX (Table 7) gave bands in the wavelength ranges of 240–380 and 660–670 nm due to $^3A_{2g} \rightarrow {}^3T_{1g}$(P) and $^3A_{2g} \rightarrow {}^3T_{1g}$(F) transitions, respectively and when gathered with the magnetic moment values (3.32 and 3.41 B.M.), a high spin octahedral structure is assigned [52]. The electronic spectral data of the yellowish-green complex X show bands at 294, 342 and 672 nm. The latter broad band is assigned to the transition $^2E_g \rightarrow {}^2T_{2g}$ (D) and is assignable to octahedral environment (Table 7). The electronic absorption spectra of the pale-green complex XI gave broad bands with maxima at 275, 380 and 600 nm. The presence of the bands at 380 and 368 nm in the copper complexes may be due to the destabilization of the energy of the lone pairs of electrons on complex formation and they are assigned to the transition $^2T_{2g} \rightarrow {}^2E_g$ of a tetrahedral structure. The slightly higher μ_{eff} values above that for the spin–orbit only arises from slight mixing of multiplete excited state in which spin–orbit coupling is appreciable. On the other hand, the spectra of the dark-green complex XII gave bands at 280, 338 and 672 nm typifying the presence of square planar stereochemistry. The white complex XIII is diamagnetic with a tetrahedral environment (μ_{eff} = zero). The nujol mull electronic absorption spectra of the yellow complex XIV gave bands at 278, 430 and 500 nm (Table 7). The strong band at 430 nm was assigned to charge transfer probably due to n–π^* transition. The band at 500 nm was attributed to $^1E_g{}^+ \rightarrow {}^2\Pi_u$ transition [53–55]. The room temperature magnetic moment, μ_{eff} value of this complex is 1.91 B.M. In general, all the data typified the existence of low spin octahedral configuration. The electronic

Table 7
Nujol mull electronic absorption spectra λ_{max} (nm), room temperature effective magnetic moment values (μ_{eff}, 298 °K) and geometries of complexes.

Complex	λ_{max} (nm)	μ_{eff}	Geometry
I	250(m),300(s),510(b)	3.85	O_h
II	310(vs),425(b),580(b)	3.87	O_h
III	353(m),570(b)	5.77	T_d
IV	230(vs),305(s),372(w),500(b)	5.91	O_h
V	235(s),310(s),550(b)	4.92	T_d
VI	255(s),305(s),600(b)	5.12	O_h
VII	300(s),540(b)	5.31	O_h
VIII	240(m),290(m),380(w),660(b)	3.32	O_h
IX	300(s),670(b)	3.41	O_h
X	294(w),342(m),724 (b)	1.85	O_h
XI	275(s),380(m),600(b)	2.11	T_d
XII	280(m),338(m),672(b)	1.98	s.p
XIV	278(s),430(b),500(b)	1.91	O_h

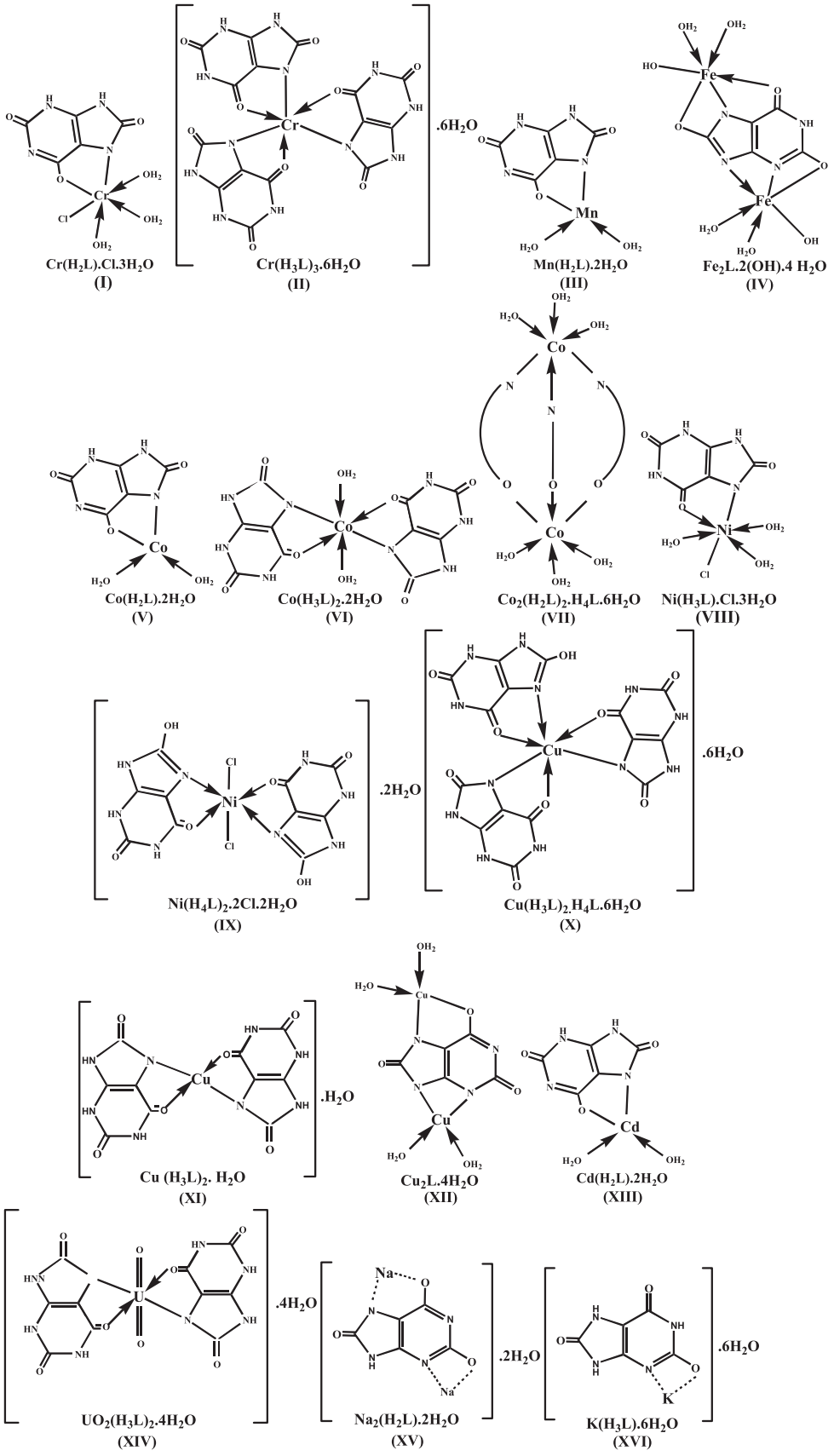

Fig. 3. The structures of the synthesized complexes.

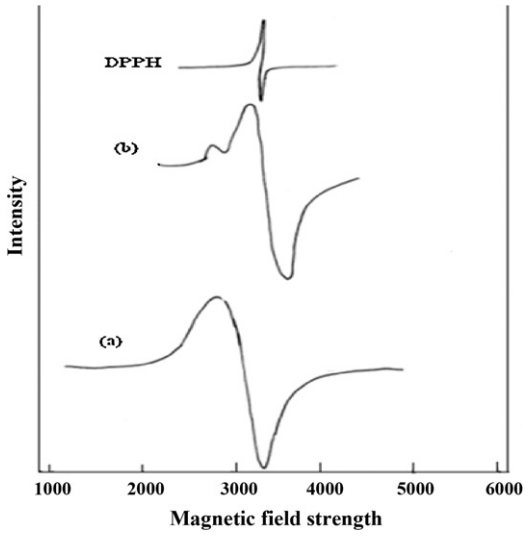

Fig. 4. X-Band ESR spectra of (a) XI and (b) X.

spectra, magnetic moment values and infrared spectra concluded the structures shown in Fig. 3.

3.4. ESR measurements

The ESR spectrum of the octahedral copper complex X showed anisotropic spectrum of an axial–elongated type (Fig. 4). It gave two g-values, $g_{//} = 2.45$ and $g_{\perp} = 2.09$. For this complex, $g_{//} > g_{\perp}$ assigns that the unpaired electron is in the $d_{x^2-y^2}$ orbital [56,57]. The room-temperature ESR spectrum of XI complex (Fig. 4) is nearly of similar spectral pattern. It is isotropic in nature with $g_s = 2.16$ and $A = 200$ ($\times 10^{-4}$). The data showed very broad signals, which may be due to the polymeric nature of these complexes. The ESR spectrum of the square–planar complex XII showed anisotropic spectrum of an axial–elongated type (Fig. 5). It gave two g-values, $g_{//} = 2.48$ and $g_{\perp} = 2.11$. The G value, 4.36, for this complex indicated strong interaction between the ligand and the metal ion. $g_{//} > g_{\perp}$ suggests that $d_{x^2-y^2}$ ground state is present [58,59]. The $\langle g \rangle$ value is calculated from the relation [60]: $[\langle g \rangle = (g_{//} + 2g_{\perp})/3]$ and equals 2.23, for this complex. The deviation of the <g> value from that of the free electron (2.0023) is due to the covalence property with a further support for tetrahedral-distorted symmetry associated with $d_{x^2-y^2}$ state rather than d_{z^2} state [13,61]. The structure can be confirmed

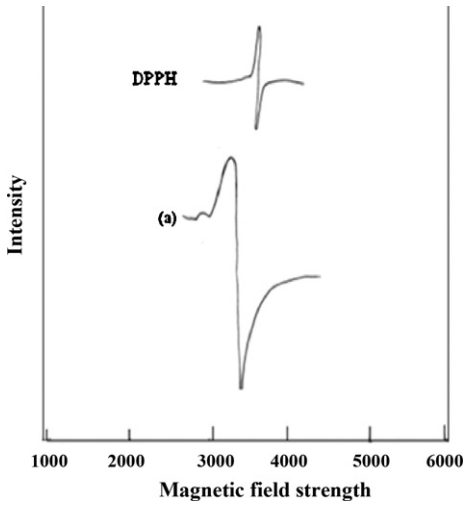

Fig. 5. X-B and ESR spectra of the complex, XII.

by nujol mull electronic spectra, IR and magnetic moment values. Generally, Cu^{II} complexes having a lower symmetry than octahedron undergo a free rotation or give complexes containing grossly misaligned tetragonal axes of magnetically dilute interaction leading to isotropic spectral feature [6]. It is possible to measure α^2, where α is the coefficient of the ground state $d_{x^2-y^2}$ orbital, from the expression [62]:

$$\alpha^2 = \frac{A_{//}}{0.036} + (g_{//} - 2.0023) + \frac{3}{7(g_{\perp} - 2.0023)} + 0.04$$

where $A_{//}$ is the parallel coupling constant expressed in cm^{-1}. The α^2 -values for Cu^{II} complexes lie in the range of 1.078–0.888 indicating that these complexes are not purely covalent in accord with the results obtained from IR and electronic spectral measurements [7,63].

3.5. Thermal analysis

3.5.1. The DTA and TGA data

The DTA data of the free ligand (Table 8) showed one broad characteristic endothermic agitation peak at 437.4 °C with activation energy of 91.87 kJ/mol and a reaction order of 0.67 which corresponds to decomposition of purine ring with the major final formation of acetonitrile. This can be proved by TGA data which gave well defined one peak. Ua contains in its structure purine ring which is believed to exhibit a high thermal stability [64]. It starts to decompose at 400 °C. The DTA and TGA data of the synthesized Ua complexes are given in Table 8 and showing a number of endothermic peaks. The data allow the following observations and conclusions:

(i) The octahedral uric acid complexes I, IV and VIII gave three well defined TGA peaks. The dehydration processes of coordinated water molecules [65] take place in the first two successive steps in the temperature range 307–579 K. The last exothermic peaks are corresponding to decomposition step with the formation of metal oxides as final products such as Cr_2O_3 [66], Fe_2O_3 and Ni_2O_3 [67]. In the temperature range 573–773 °C, four DTA peaks overlapped with each other gave one TGA step which corresponds to decomposition of the ligand and formation of Fe_2O_3.

(ii) From TGA data, the complex V gave three well defined peaks. The dehydration of coordinated water molecules takes place in the first step only in the temperature range 305–421 K. The last two exothermic peaks are corresponding to decomposition step and formation of the basic cobalt cyanide, Co(OH)CN as a final product [10].

(iii) The octahedral complex XIV gave four well defined TGA peaks (Fig. 6 and Table 8). The dehydration processes of lattice water molecules [65] take place in the first two successive steps in the temperature range 343–589 K. The last two steps are due to thermal agitation with formation of UO_2 as a final product. The DTA curves confirm these results which gave four peaks.

The calculated activation energy, E_a, entropy of activation, $\Delta S^{\#}$ and the change in enthalpy, $\Delta H^{\#}$ for any phase transformation are collected in Table 8. The change of entropy, $\Delta S^{\#}$, values for all complexes are nearly of the same magnitude and lie within the range from (−0.28) to (−0.32) kJ K^{-1} mol^{-1}. It is concluded that the transition states are more ordered, i.e. in a less random molecular configuration than the reacting complex. The fraction appeared in the calculated order of the thermal reaction, n, also confirms that the reactions proceeded in complicated mechanisms. The calculated values of the collision number, z showed a direct relation to E_a.

Table 8
DTA analysis of Uric acid (H_4L) and their metal complexes.

Compound	Type	T_m (°K)	E_a (kJ mol^{-1})	n	α_m	$\Delta S^{\#}$ (kJ K^{-1} mol^{-1})	$\Delta H^{\#}$ (kJ mol^{-1})	10^3 (ZS^{-1})	T (°C) TGA	Wt. loss (%)		Assignment
										Calcd. (%)	Found. (%)	
Ua	Endo	710	91.87	0.67	0.702	−0.306	−217.3	0.015	358.9–493.6	75.54	76.03	Decomposition of purine ring and formation of acetonitrile
I	Endo	353	95.83	1.16	0.605	−0.294	−103.8	0.032	35.9–175.7	20.64	15.95	Dehydration of 1.5 coordinated water molecules and HCl
	Endo	385	313.67	1.65	0.537	−0.286	−109.9	0.097				
	Endo	505	133.24	1.26	0.589	−0.297	−150.0	0.031	175.7–260.0	8.77	5.99	Loss of 1.5 coordinated H_2O molecules
	Exo	649	271.52	1.11	0.613	−0.295	−191.7	0.050	260.0–441.4	52.06	42.33	Decomposition of the rest ligand and formation of Cr_2O_3
IV	Endo	453	209.02	1.58	0.546	−0.291	−132.1	0.055	83.0–197.4	6.99	6.59	Loss of 1.5 coordinated water molecules
	Exo	525	142.91	1.41	0.568	−0.297	−156.1	0.033	197.4–306.0	11.66	12.00	Loss of 2.5 coordinated H_2O molecules
	Exo	633	404.23	0.89	0.653	−0.291	−184.6	0.076	306.0–495.5	38.87	46.84	Decomposition of the rest ligand and formation of Fe_2O_3
	Exo	655	405.83	1.84	0.516	−0.292	−191.4	0.075				
	Exo	704	1129.69	1.62	0.541	−0.284	−200.8	0.193				
	Exo	757	19.12	1.31	0.582	−0.320	−242.3	0.003				
V	Endo	358	38.08	1.26	0.589	−0.302	−108.1	0.012	33.4–173.3	13.68	14.21	Removal of two coordinated water
	Exo	613	297.92	1.36	0.574	−0.294	−180.0	0.058	173.3–448.2	41.81	42.23	Elimination of 2HCN and 2CO
									550.0–731.0	5.32	4.72	Elimination of $0.5N_2$ and formation of Co(OH)CN
VIII	Endo	358	65.82	0.93	0.646	−0.297	−106.4	0.022	34.4–140.0	14.22	14.59	Dehydration of $2.5H_2O$ coordinated molecules
	Endo	385	299.04	1.78	0.522	−0.286	−110.1	0.093				
	Endo	406	375.28	1.43	0.565	−0.285	−115.7	0.111				
	Endo	463	140.88	1.21	0.596	−0.295	−136.7	0.036	140.0–264.6	14.37	10.83	Loss of 0.5 H_2O + HCl
	Exo	528	45.27	1.26	0.589	−0.307	−162.0	0.010	264.6–462.5	44.88	34.68	Loss of N_2, 2HCN, 1.5C, 1.5CO and formation of Ni_2O_3
	Exo	608	388.86	1.14	0.608	−0.291	−177.1	0.076				
	Exo	703	305.71	1.44	0.563	−0.296	−207.9	0.052				
XII	Endo	377	15.89	1.22	0.596	−0.309	−116.8	0.005	31.8–148.0	12.35	10.49	Dehydration of 2.5 coordinated H_2O
	Exo	491	227.68	1.02	0.629	−0.292	−143.5	0.056	148.0–335.8	33.75	29.75	Elimination of 1.5 H_2O, 2CO, N_2, C and formation of basic copper cyanide
	Exo	625	434.64	1.26	0.589	−0.291	−181.8	0.084				
	Exo	663	467.67	1.11	0.613	−0.291	−193.1	0.085				
XIV	Endo	383	28.39	0.85	0.661	−0.305	−116.9	0.009	70.2–189.0	6.63	6.84	Dehydration of 2.5 outer sphere H_2O
	Endo	478	35.34	1.93	0.507	−0.307	−146.8	0.009	189.0–316.7			Dehydration of 1.5 outer sphere H_2O
	Exo	653	295.66	0.95	0.641	−0.295	−192.4	0.055	316.7–477.9	40.78	42.48	Loss of 4HCN, N_2, 5CO
	Exo	730	545.14	1.36	0.574	−0.292	−212.8	0.089	477.9–564.5	8.55	8.98	Decomposition of the rest ligand and formation of UO_2

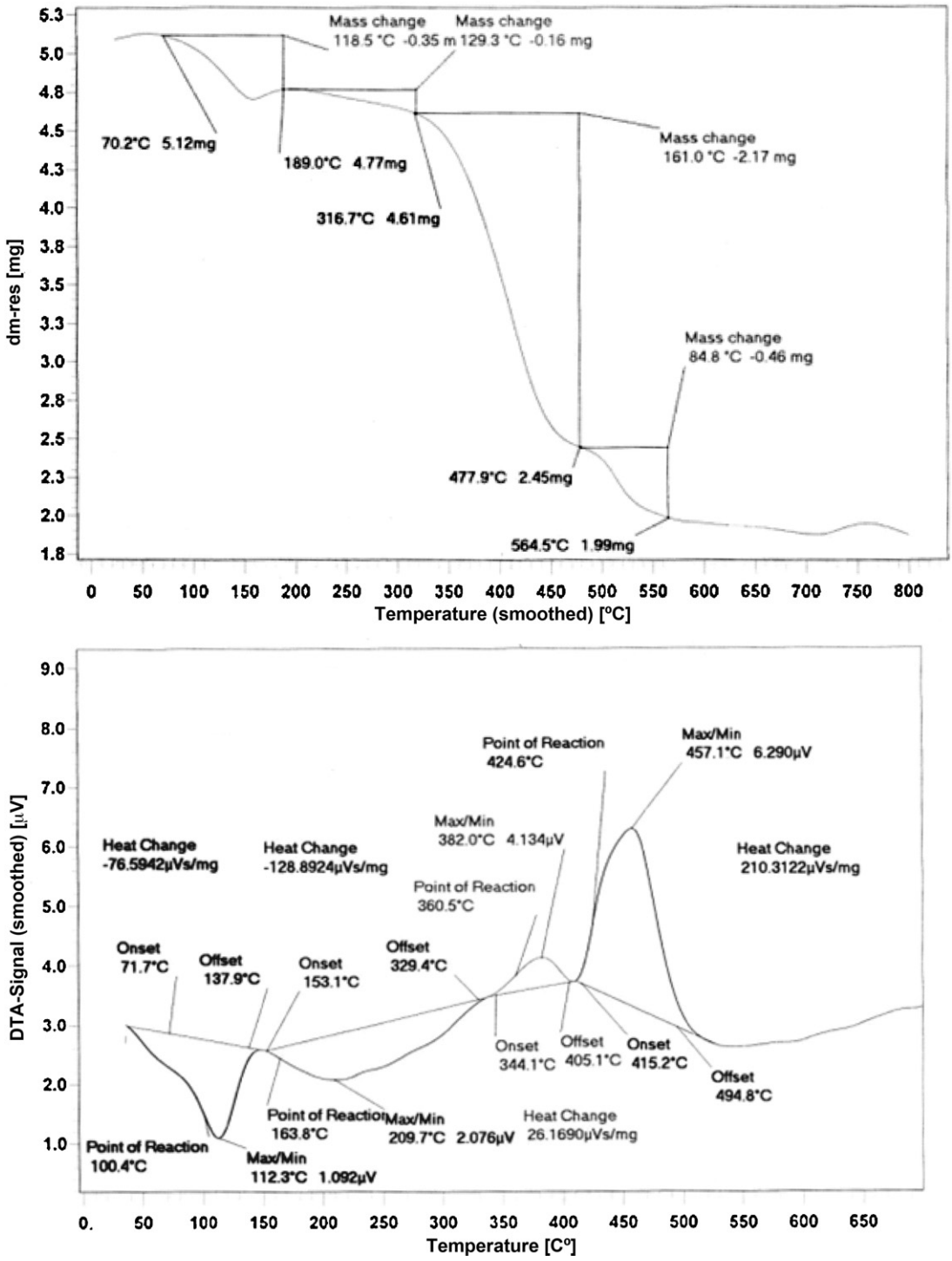

Fig. 6. TGA and DTA curves of the complex XIV.

3.5.2. *Differential scanning calorimetry, DSC*

DSC is a technique used to study the thermal transitions of a compound such as glass transition, melting and crystallization. Plotting heat flow against temperature gave three regions. In the first region, glass transition temperature can be determined by taking the middle of the incline, in the second region, it can be determined by taking the temperature at the lowest point of the dip and in the third region, melting temperature can be determined by taking the temperature at the top of the peak. Thermal transition of Ua and their complexes are collected in Table 9. Ua has no glass transition temperature since there are no thermal changes

Table 9
Thermal transitions of uric acid (H_4L^1) and some complexes.

Compound	Thermal transitions (°C)		
	T_g	T_c	T_m
Ua	–	435.6	457.0
I	104.0	210.0	365.5
IV	100.6	248.7	386.0
V	88.6	153.9	313.1
VIII	70.8	146.7	416.8
XII	95.5	214.0	380.2
XIV	129.7	189.1	458.7

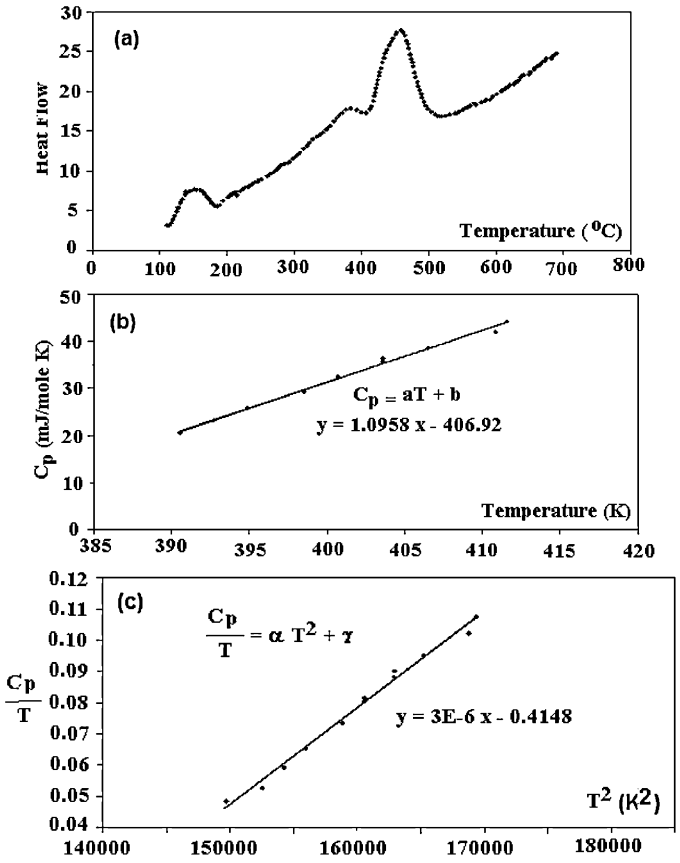

Fig. 7. DSC curves for the complex XIV: (a) dependence of heat flow on temperature, (b) dependence of specific heat on temperature, and (c) variation of C_p/T versus T^2.

until 417.3 °C i.e. it decomposes at higher temperature. The glass transition temperature for all complexes can be determined from DSC graph since they exhibit dehydration process due to lattice and coordinated water molecules followed by thermal agitation decomposition. This is compatible with the explanation of TGA for these complexes. The complex XIV has the highest value of T_g (Table 9 and Fig. 7) where this complex contains two molecules of Ua forming an octahedral geometry with two water molecules. The crystallization temperature of Ua is 435.6 in which it will gain enough energy to move into very ordered arrangements and then it gives off heat through an exothermic transition. DSC plot is used to carefully determine the melting temperature through an endothermic transition and thus, Ua must absorb heat until all the crystals have melted. Melting temperature of Ua and their complexes are ranged between 233.5 and 458.0 °C. From DSC also, the heat capacity can be determined by dividing the heat flow by the heating rate. The variation of C_p versus T can be represented using Debye model according to the following relations

$$C_p = aT + b \quad \frac{C_P}{T} = \alpha T^2 + \gamma$$

where a and α are slopes, b and γ are intersection. By applying this model to the complex XIV (Fig. 7) the first part represent dependence of heat flow on temperature. From this curve, glass transition crystallization and melting temperature can be determined. The second part represents the dependence of specific heat on temperature while the third part shows the variation of C_p/T with T^2.

3.6. Biological activity

Eight microorganisms representing different microbial categories, three Gram-positive (*Bacillus subtilis*, *Streptococcus penumonia* and *Staphylococcus aureas*) and two Gram negative (*Escherichia coli* and Pesudomonas sp.) bacteria and three yeasts (Candida, *Aspergillus nigaer* and penicillium sp.) were used to study the biological activity of Ua and ten of its complexes. The data allow the following observations and conclusions (Table 10):

1. The metal complexes have higher activity [66,67] than the free ligand. Such increased activity of the metal chelates could be explained on the basis of overtones concept and chelation theory [68]. The cell permeability, the lipid membrane that surrounds the cell, favors the passage of only lipid soluble materials on the basis that liposolubility is an important factor that controls antimicrobial activity. On chelation, the polarity of the metal ion is reduced to a greater extent due to the overlap of the ligand orbital and partial sharing of the positive charge of the metal ion with the donor groups. Furthermore, it increases the delocalization of p- and d-electrons over the whole chelate and enhances the lipophilicity of the complex. The increased lipophilicity enhances the penetration of the complexes into lipid membranes and blocking of metal binding sites on the enzymes of the microorganism.
2. The complexes of square planar geometry exhibited antimicrobial activity such as observed for complex XII. Accordingly, the antimicrobial activity of the complex seems to be highly affected by its structural geometries [69].
3. Generally, the studied complexes have higher activity for Gram (+) than for Gram (−) bacteria (Table 10). The highest active compound for Gram (−) bacteria is octahedral complex IV while square planar complex XII is the highest active for Gram (+) bacteria. On the other hand, most compounds showed higher antifungal activity.
4. Because the metal complexes have higher activities than the free ligands, one can say that many drugs may possess modified pharmacological and toxicological properties when administered in the form of metallic complexes [70]. Probably the most widely studied cation in this respect is Cu(II), since many copper complexes have been proven beneficial against several diseases such as tuberculosis, rheumatoid, gastric ulcers and cancers [70–73].
5. Compounds with noticeable activity may be considered as a start point for development of some new antimicrobial activity.

Generally, the biological activities of the complexes can be arranged as: tetrahedral > square planar > octahedral complexes and this may be attributed to the steric hindrance of the ligands in Oh field.

3.7. Optimal conditions for formation of the urate complexes

Uric acid reacts with trivalent iron to form a brown complex. The effect of pH on the absorption spectra of Fe(III)–ligand mixture was studied by mixing 1×10^{-4} M of the metal ions with 3×10^{-4} M ligand under a controlled pH values. The pHs were adjusted using portions of 0.1 M HNO_3 and 0.1 M KOH and the absorbance values of the solutions were measured in the range of λ = 300–500 nm. It is evident from the results, the absorbance gave maximum value at pH 3.5 for Fe(III)–ligand mixture at $\lambda_{max} = 350$ nm. The validity of Beer's law checked under the optimum condition gave good straight line and the molar absorpitivity were calculated for the mixture at different λ_{max} (Fig. 8).

Table 10
Biological activities of ligands and some of their complexes.

	G+ bacteria			G− bacteria		Yeast		
	Bacillus subtilis	*Streptococcus penumonia*	*Staphylococcus aureas*	*E. coli*	Pesudomonas Sp	Candida	*Aspergillus nigaer*	Penicillium Sp
Ua	+	–	+	+	+	–	–	+
II	++	+++	+	+++	+	+	+++	++
III	++	+++	+++	++	+	+	+++	++
IV	+	+++	++	+++	+++	+	+++	+
V	++	–	–	+	+++	–	+	+
VIII	+++	++	+++	+	++	+	++	+++
XII	+++	+++	+++	+	+	++	–	+++
XIII	++	+++	+	–	+	+	+++	+
XIV	+	+	–	–	+	++	+	+
XV	++	+++	+	+++	+	+++	–	+
XVI	–	+	++	+	+	+++	+	++

(–) inactive, (++) moderately active, (+) slightly active, (+++) highly active.

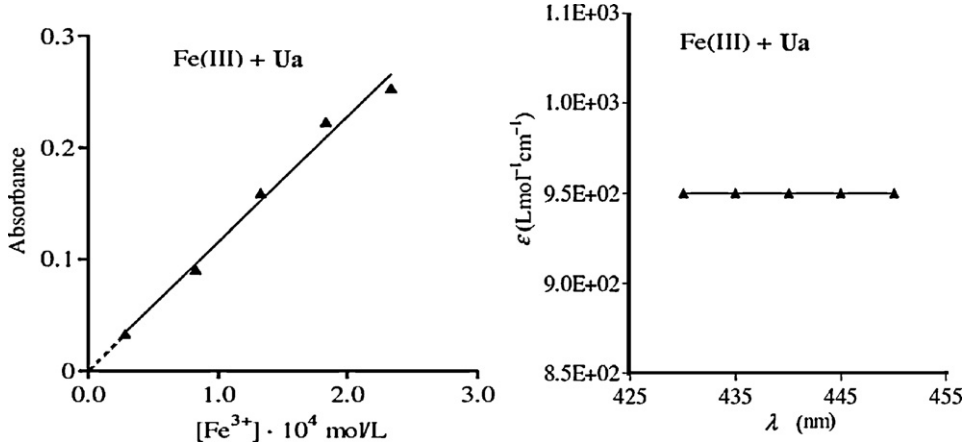

Fig. 8. Confirmation of the Beer's law for the $Fe(Ua)_n$ complex.

3.7.1. The molar ratio method

When Fe^{3+} reacts with Ua, it gives the colored complex $Fe(Ua)_n$. if the concentration of Fe^{3+} is kept constant while that of Ua is varied, the absorbance of the complex, A_s will equal: $A_s = \varepsilon \ell [Fe(Ua)_n]$. It is assumed that Beer's law is obeyed and ε is the molar extinction coefficient, ℓ is the cell thickness in cm. Some of the graphs plotted for the molar ratio method were shown in Fig. 9.

As the concentrations of the ligand increases, the bands become more intense. The position of λ_{max} for the iron–uric acid system is 350 nm. The stoichiometry of the reaction is obtained by plotting the absorbance of the resultant solution against the molar ratio of the variable concentration of the ligand to the constant concentration of the metal. If the system forms a stable complex which does not show appreciable dissociation, such a plot gives a sharp break which corresponds to the stoichiometry of this complex. Linear extrapolation of the curve is made where the curved plot becomes parallel to the molar ratio axis after the addition of an excess of the variable component. The data indicated that the composition of the formed complex, $Fe(Ua)_n$ is 1:2 and 1:6 (metal ions:ligand) (Fig. 10 and Table 11).

3.7.2. The straight line method

When Fe^{3+} reacts with *Ua*, it gives the colored complex $Fe(Ua)_n$. The dissociation constant K_d can be calculated as follows:

$$K_d = \frac{[Fe^{3+}][Ua]^n}{[Fe(Ua)_n]}$$

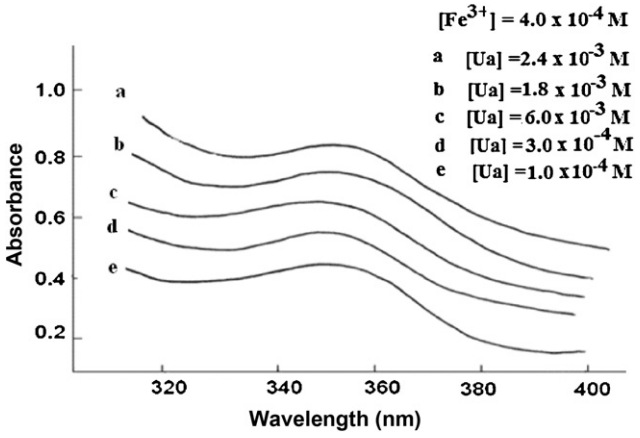

Fig. 9. Determination of the $Fe(Ua)_n$ complex by molar ratio method.

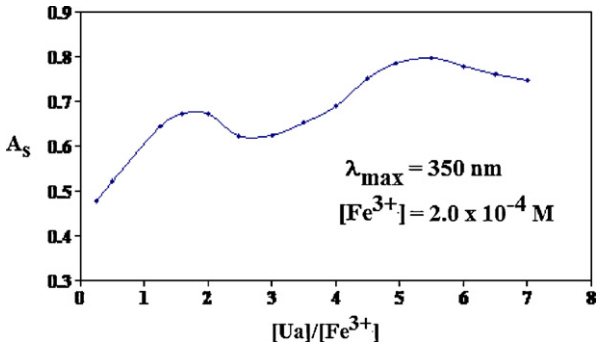

Fig. 10. Molar ratio plot for iron–uric acid reaction.

Table 11
pKa values and the stoichiometry of iron–uric acid complex using different spectrophotometric methods.

Methods	Fe–uric-acid	pKa
Molar ratio	1:2,1:6	–
Straight line (simple plot)	1:1, 1:2, 1:3	–
Straight line (logarithmic plot)	1:1	7.70
Continuous variation	1:2	4.85
Slope ratio	1:1	–
Limiting logarithmic	1:1	–

The equilibrium concentrations, $[Fe^{3+}]_e$ and $[Ua]_e$ can be calculated as follows:

$$[Fe^{3+}]_e = [Fe^{3+}] - [Fe(Ua)_n]$$
$$[Ua]_e = [Ua] - n[Fe(Ua)_n]$$
$$[Ua]_e = [Ua] - n([Fe^{3+}] - [Fe^{3+}]_e)$$

Applying Beer–Lamberts law (ℓ =1 cm):

$$[Fe(Ua)_n] = \frac{A_s}{\varepsilon}$$

By mathematical treatment of the above equation, it is concluded that:

$$\frac{1}{V^n} = \frac{CD}{K_d A_s} - \frac{D}{K_d}$$

Where

$$C = \frac{[Fe^{3+}]_o \varepsilon V_o}{V}$$

and

$$D = \left(\frac{[Ua]_o V_o}{V}\right)^n$$

The straight-line method carried out using constant [Fe^{3+}] at 4.0×10^{-4} M while the [Ua] varied within the range 1×10^{-4}–3.0×10^{-3} M and the pH of solution was adjusted at optimum value. The plot of $(1/V)^n$ vs. $1/A_s$, where (n = 1, 2, 3) gave a linear relationship (Fig. 11) if the value of n is the same as in the equilibrium equation.

This is valid in cases of n = 1, 2 and 3 to point to the formation of 1:1, 1:2 and 1:3 species for iron–uric acid complexes (Table 11). Thus, a series of complexes in equilibrium to each other were formed. If the complex is strongly dissociated: $K_d/DV^n \gg 1$and thus:

$$A_s = \frac{CDV^n}{K_d}$$

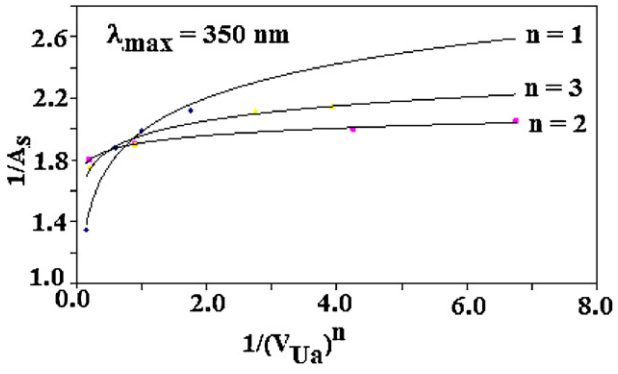

Fig. 11. Determination of the stoichiometry of $Fe(Ua)_n$ complex by straight-line method.

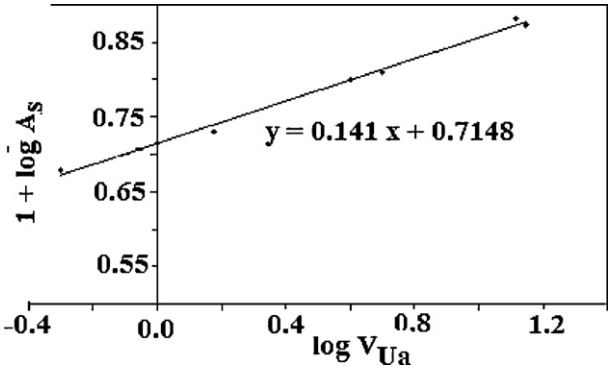

Fig. 12. Straight line logarithmic plot for iron–uric acid reaction.

$$\log A_s = \log \frac{CD}{K_d} + n \log V$$

Plotting $\log A_s$ vs. $\log V$ gave a straight line from which the values of n and $\log CD/K_d$ can be derived from the slope and intercept, respectively (Fig. 12). Therefore, the equilibrium constant and the stoichiometry of the complexes can be evaluated. The data verified the stoichiometry of 1:1 iron–uric acid complex (Table 11).

3.7.3. The continuous variation method (Job's method)

To determine n for $Fe(Ua)_n$, solutions of [Fe^{3+}] and [Ua] of the same molar concentrations are mixed in varying proportions so the total number of moles of Fe^{3+} and Ua together are always constant. The difference between the absorbance value measured and the value for no reaction is plotted against the mole fraction of Fe^{3+} and Ua. The resulting curve should have a maximum if the property measured has a larger value for the complex than for Fe^{3+} and Ua, or a minimum if this property is smaller. Sometimes the determination of the stoichiometry of formed complexes is wavelength dependent. It was pointed out that the continuous variation method should not give a maximum as an indication for the complex. But, however, the appearance of a shoulder in the curve might be taken as an indication for the existence of a complex having the corresponding composition. The data was recorded at 350 nm (Fig. 13), for iron–uric acid complex.

The absorbance-mole fraction plots are of broad feature where dissociation of these complexes is suggested with iron–uric acid. If the concentration of $Fe(Ua)_n$ is C and its absorbance would be the same as the absorbance A_m which is the limiting absorbance reached when large excess of Ua presents in solution. Actually, the formation of complexes is not quite complete at the end point and thus absorbance of Fe^{3+} at that point is smaller than A_m and can be calculated by taking the intersection value of the two straight

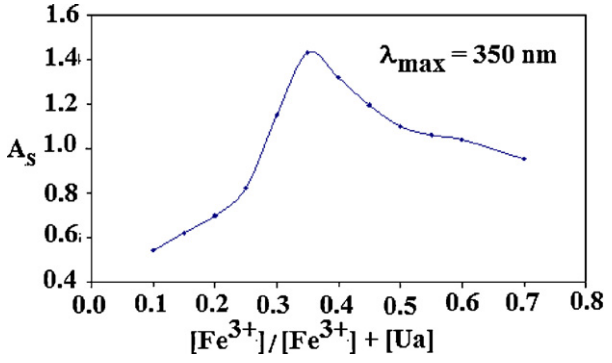

Fig. 13. Determination of the stoichiometry of $Fe(Ua)_n$ complex by continuous variation method.

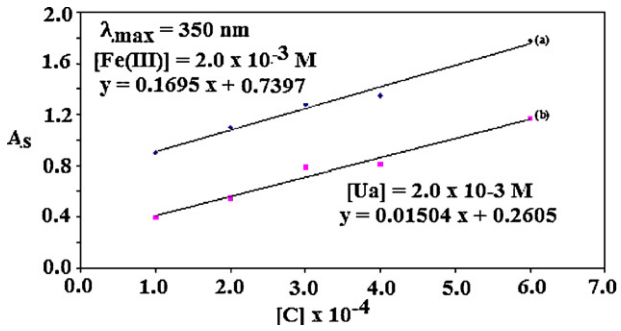

Fig. 14. Slope-ratio method for iron–uric acid reaction in aqueous media. (a) Variable uric acid concentration. (b) Variable Fe concentration.

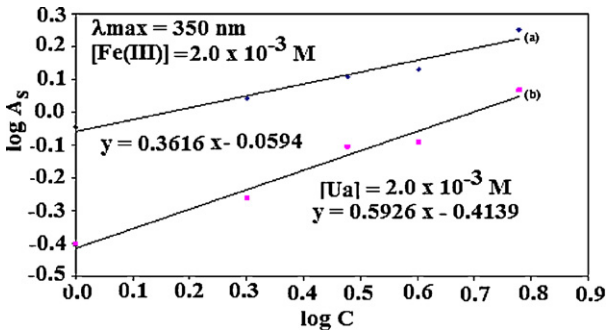

Fig. 15. limiting logarithmic method for iron–uric acid reaction in aqueous media. (a) Variable uric acid concentration. (b) Variable Fe concentration.

lines. For calculating the dissociation constant of a complex of the type $Fe(Ua)_2$, where C is the initial concentration and $K_{1:2}$ is the equilibrium constant:

$$[Fe(Ua)_2] = C\left(\frac{A}{A_m}\right)$$
$$[Fe^{2+}] = C\left(\frac{1-A}{A_m}\right)$$

and

$$[Ua^-] = 2C\left(\frac{1-A}{A_m}\right)$$

$$K_{1:2} = \frac{[Fe^{2+}][Ua^-]^2}{[Fe(Ua)_2]}$$
$$K_{1:2} = \frac{4C^2(1-A/A_m)}{(A/A_m)}$$

The results confirmed the composition of the formed complex as 1:2 (Table 11).

3.7.4. The slope ratio method

When m moles of Fe^{3+} react with n moles of Ua, the complex $Fe_m(Ua)_n$ is formed. If the concentration of Ua is kept constant and in sufficient excess to make dissociation negligible, the equilibrium concentration of the complex $Fe_m(Ua)_n$ will be essentially proportional to the analytical concentration of Fe^{3+} added in the reaction, thus: $[Fe_m(Ua)_n] = C_{Fe^{3+}}/m$

By applying in Beer's law:

$$A_s = \varepsilon\ell\left(\frac{C_{Fe^{3+}}}{m}\right)$$

If absorbance is plotted against different analytical concentrations of Fe^{3+}, keeping the concentration of Ua constant and in excess, a straight line is obtained with a $(slope)_1$ of $\varepsilon\ell/m$. Similarly, if the concentration of Fe^{3+} is kept constant in excess and the concentration of Ua is varied so that:

$$[Fe_m(Ua)_n] = \frac{C_{Ua}}{n}$$

and accordingly

$$A_s = \varepsilon\ell\left(\frac{C_{Ua}}{n}\right)$$

a straight line is obtained when absorbance is plotted against different analytical concentrations of Ua, keeping the concentration of Fe^{3+} constant with $(slope)_2$ of $\varepsilon\ell/n$. Therefore,

$$\frac{(slope)_1}{(slope)_2} = \frac{n}{m}$$

The absorbance of the two sets of solutions was measured at λ_{max} = 350 nm (Fig. 14).

It was found that the data obtainable from this method confirms the stoichiometry 1:1 for iron–uric acid complex.

3.7.5. The limiting logarithmic method

The limiting logarithmic method was based on the same mode of thinking given for the slope ratio method by plotting the logarithmic values of the absorbance versus the logarithmic values of the variable concentrations (Fig. 15).

The stoichiometry of the complex reaction is assigned based on the ratio of the slopes of the two straight lines obtained. It was found that the data obtainable from this method confirms the stoichiometry 1:1 for iron–uric acid complex.

3.7.6. The successive method

This method was constructed depending on the changes of both the concentrations of the ligand and the metal ion. So, the stability constant of the formed complex can be calculated. When m moles of Fe^{3+} react with n moles of Ua, the complex $Fe_m(Ua)_n$ is formed. The charge on the complex could be determined by knowing the values of n and m. However, these values are omitted for simplicity. The concentrations of Fe^{3+} and Ua^- can be calculated as follows:

$$C_{Fe} = [Fe] + [Fe(Ua)_n]$$

$$C_{Ua} = [HUa] + [Ua^-] + [Fe(Ua)_n]$$

If β is the stability quotient of $Fe_m(Ua)_n$ and K_a is the dissociation of the ligand, it may be shown that:

$$HUa \leftrightarrow H^+ + Ua^-, \quad K_a = \frac{[H^+][Ua^-]}{[HUa]}$$

$$Fe^{3+} + Ua^- \leftrightarrow Fe(Ua)_n, \quad \beta = \frac{[Fe(Ua)_n]}{[Fe^{3+}][Ua^-]}$$

From these two equations, the following equation is deduced:

$$\frac{\beta}{1+([H^+]/K_a)} = \frac{[Fe(Ua)_n]}{[Fe^{3+}]([HUa]+[Ua^-])}$$

If the reaction is measured at constant pH, the left-hand side of the above equation is constant and symbolized by q. By applying Beer's law for 1 cm optical path length:

$$C_{complex} = \frac{A_s}{\varepsilon}$$
$$[Fe^{3+}] = C_{Fe^{3+}} - C_{complex}$$
$$[Ua^-] = C_{Ua^-} - C_{complex}$$

So, the q value becomes:

$$q = \frac{(A_s/\varepsilon)}{(C_{Fe^{3+}} - (A_s/\varepsilon))(C_{Ua^-} - (A_s/\varepsilon))}$$

Table 12
The molecular extinction ε and the formation constant q for iron–uric acid complex.

Iron–uric acid complex at λ=285 nm	ε	q
	23228.9	27718

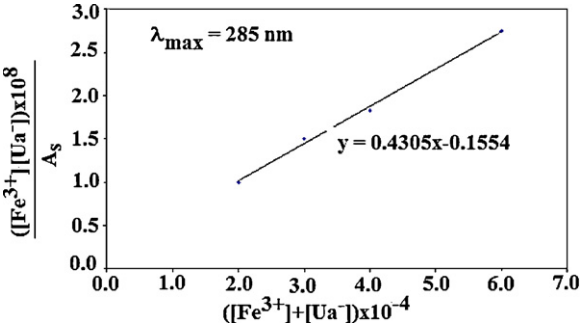

Fig. 16. Successive method for iron–uric acid reaction.

Where A_s is the absorbance due to $Fe_m(Ua)_n$, ε is the molar extinction coefficient of the formed complex.

$$q = \frac{(A_s/\varepsilon)}{C_{Fe^{3+}}C_{Ua^-} + (A_s/\varepsilon)^2 - A_s/(C_{Fe^{3+}} + C_{Ua^-})}$$

The value $(A_s/\varepsilon)^2$ is neglected with no appreciable error so that:

$$\frac{1}{q\varepsilon} = \frac{C_{Fe^{3+}}C_{Ua^-} - [(A_s(C_{Fe^{3+}} + C_{Ua^-})/\varepsilon}{A_s}$$

$$\frac{C_{Fe^{3+}}C_{Ua^-}}{A_s} = \frac{1}{q\varepsilon} + \frac{(C_{Fe^{3+}} + C_{Ua^-})}{\varepsilon}$$

The plot of the left-hand side of the above equation, $C_{Fe^{3+}}C_{Ua^-}/A_s$ versus $(C_{Fe^{3+}} + C_{Ua^-})$ gave a straight line with a slope equals to $1/\varepsilon$ and an intercept of $1/q\varepsilon$. The values of the overall formation constant and the molecular extinction coefficients for this system are collected in Table 12 and Fig. 16. The reported stoichiometry for the iron barbituric acid complexes[13] are 1:1 and 1:3. However, in case of the iron–uric acid, the stoichiometries are 1:1, 1:2, 1:3 and 1:6. This means that uric acid has high reactivity to chelate with iron to form different stoichiometries more than in barbituric acid.

4. Conclusion

Uric acid, as one of biologically active compound formed in the human body, makes an important interaction with transition metal ions to form complexes. These complexes have different geometries and possess biological activities more than uric acid itself.

References

[1] M. Soriani, D. Pietraforte, M. Minetti, Antioxidant potential of anaerobic human plasma: role of serum albumin and thiols as scavengers of carbon radicals, Arch. Biochem. Biophys. 312 (1994) 180–188.
[2] M.G. Simic, S.V. Jonanovic, Antioxidation mechanisms of uric acid, J. Am. Chem. Soc. 111 (1989) 5778–5782.
[3] G. Wessman, G.A. Rita, Molecular basis of gouty inflammation: interaction of monosodium urate crystals with lysosomes and liposomes, Nature New Biol. 240 (1972) 167–172.
[4] M.S. Masoud, A. El-Dissouky, E.E. Ghatwary, Synthesis and stereochemistry of new cobalt azo-nitroso complexes, Inorg. Chim. Acta 141 (1988) 119–123.
[5] M.S. Masoud, S.A.A. Ali, G.Y. Ali, I.M. Abed, Thermodynamic parameters of ionization of 5-(2-substituted phenylazo) barbituric acids, Thermochim. Acta 122 (1987) 209–220.
[6] M.S. Masoud, A.K. Ghonaim, R.H. Ahmed, S.A. Abou El-Enein, A.A. Mahmoud, Ligating properties of 5-nitrobarbituric acid, J. Coord. Chem. 55 (2002) 79–105.
[7] M.S. Masoud, A.A. Soayed, A.E. Ali, O.K. Sharsherh, Synthesis and characterization of new azopyrimidine complexes, J. Coord. Chem. 56 (2003) 725–742.
[8] M.S. Masoud, A.E. Ali, M.A. Shaker, M. Abdul Ghani, Solvatochromic behavior of the electronic absorption spectra of some azo derivatives of amino pyridines, Spectrochim. Acta 60A (2004) 3155–3159.
[9] M.S. Masoud, S.A. Abou El-Enein, M.E. Ayad, A.S. Goher, Spectral and magnetic properties of phenylazo-6-aminouracil complexes, Spectrochim. Acta 60A (2004) 77–87.
[10] M.S. Masoud, E.A. Khalil, A.M. Hindawey, A.E. Ali, E.F. Mohamed, Spectroscopic studies on some azo compounds and their cobalt, copper and nickel complexes, Spectrochim. Acta 60A (2004) 2807–2817.
[11] M.S. Masoud, E.A. Khalil, A.M. Ramadan, Thermal properties of some CoII, NiII and CuII complexes of new substituted pyrimidine compounds, J. Anal. Appl. Pyrolysis 78 (2007) 14–23.
[12] M.S. Masoud, A.A. Ibrahim, E.A. Khalil, A. El-Marghany, Spectral properties of some metal complexes derived from uracil-thiouracil and citrazinic acid compounds, Spectrochim. Acta 67A (2007) 662–668.
[13] M.S. Masoud, E.A. Khalil, A.M. Ramadan, Y.M. Gohar, A. Sweyllam, Spectral, electrical conductivity and biological activity properties of some new azopyrimidine derivatives and their complexes, Spectrochim. Acta 67A (2007) 669–677.
[14] M.S Masoud, M.F. Amira, A.M. Ramadan, G.M. El-Ashry, Synthesis and characterization of some pyrimidine, purine, amino acid and mixed ligand complexes, Spectrochim. Acta 69A (2008) 230–238.
[15] H.H. Hammud, K.T. Holman, M.S. Masoud, A. El-Faham, H. Beidas, 1-Hydroxybenzotriazole (HOBt) acidity, formation constant with different metals and thermodynamic parameters: synthesis and characterization of some HOBt metal complexes – crystal structures of two polymers: $[Cu_2(H_2O)_5(OBt)_2(\mu\text{-}OBt)_2]\cdot 2H_2O\cdot EtOH$ (1A) and [Cu(μ-OBt)(HOBt)(OBt) (EtOH)] (1B), Inorg. Chim. Acta 362 (2009) 3526–3540.
[16] G. Schwarzenbach, Complexometric Titration, Methuen Co, London, 1957, Translated by H. Irving.
[17] A.I. Vogel, A Text Book of Quantitative Inorganic Analysis, Longman, London, 1978.
[18] R.H. Lee, E. Griswold, J. Kleinberg, Studies on the stepwise controlled decomposition of 2,2′-bipyridine complexes of cobalt(II) and nickel(II) chlorides, Inorg. Chem. 3 (1964) 1278–1283.
[19] B.N. Figgis, J. Lewis, Modern Coordination Chemistry, Interscience, New York, 1967, p. 403.
[20] J.M. Hernando, O. Montero, C. Blanco, The correlation of the stability constants of 1,3-dicarbonylic monochelates of Iron (III) with the acid dissociation constants of the ligand, J. Solid Chem. 19 (1990) 1191–1197.
[21] A. Holme, F.J. Langmyhr, A modified and a new straight-line method for determining the composition of weak complexes of the form A_mB_n, Anal. Chim. Acta 36 (1966) 383–391.
[22] N. Mahadevan, R.M. Sathe, Ch. Venkateswarlu, Spectrophotometric study of complexes of titanium with sulphosalicylic acid and EDTA using auxiliary complexing agents in the job's method, J. Inorg. Nucl. Chem. 25 (1963) 1005–1010.
[23] K.C. Ingham, On the application of Job's method of continuous variation to the stoichiometry of protein–ligand complexes, Anal. Biochem. 68 (1975) 660–663.
[24] A.K. Majumdar, C.P. Savariar, Spectrophotometric determination of iron with 2-hydroxy-3-napthoic acid, Anal. Chim. Acta 21 (1959) 47–52.
[25] M. Atanasov, K. Petrov, E. Mirtcheva, C. Friebel, D. Reinen, Cation distribution and coordination chemistry of Cu(II) in Zn(II) hydroxide nitrate solid solutions: a structural and spectroscopic study, J. Solid State Chem. 118 (1995) 303–312.
[26] T. Kennedy, R.S. Sinclair, T.J. Sinclair, The U.V. spectrum and photolysis of phosphorus halides in hydrocarbon solvents – II phosphorus tribromide and phosphorus pentabromide in cyclohexane, J. Inorg. Nucl. Chem. 33 (1971) 2369–2376.
[27] Y. Dong, H. Fujii, M.P. Hendrish, R.A. Leising, G. Pan, C.R. Randall, E.C. Wilkinson, Y. Zang, L. Que, B.G. Fox, K. Kauffmann, E. Munck, A High-valent nonheme iron intermediate. Structure and properties of $[Fe_2(.mu.\text{-}O)_2(5\text{-}Me\text{-}TPA)_2](ClO_4)_3$, J. Am. Chem. Soc. 117 (1995) 2778–2792.
[28] D. Frenkel, B. Smit, Understanding Molecular Simulation: From Algorithms to Applications, Academic Press, San Diego, 1996, ISBN 0-12-267370-0.
[29] A.R. Leach, Molecular Modelling: Principles and Applications, Prentice Hall, Englewood Cliffs, N.J., 2001, ISBN 0-582-38210-6.
[30] T.V. Timofeeva, V.N. Nesterov, M.Y. Antipin, R.D. Clark, M. Sanghodasa, B.H. Cardelino, C.E. Moore, D.O. Frazier, Molecular modeling and experimental study of non-linear optical compounds: monosubstituted derivatives of dicyanovinylbenzene, J. Mol. Struct. 519 (2000) 225–241.
[31] M.S. Masoud, A. El-Merghany, M.Y. Abd El-Kaway, Synthesis and physicochemical properties of biologically active purine complexes, Synth. React. Inorg. Met. Org. Nano-Met. Chem. 39 (2009) 537–553.
[32] R.M. Issa, M.K. Awad, F.M. Atlam, Quantum chemical studies on the inhibition of corrosion of copper surface by substituted uracils, Appl. Surf. Sci. 255 (2008) 2433–2441.
[33] S. Sagdinc, B. Köksoy, F. Kandemirli, S.H. Bayari, Theoretical and spectroscopic studies of 5-fluoro-isatin-3-(N-benzylthiosemicarbazone) and its zinc(II) complex, J. Mol. Struct. 917 (2009) 63.
[34] K. Fukui, Theory of Orientation and Stereoselection, Springer-Verlag, New York, 1975.
[35] Y. Gong, J. Liu, W. Tang, C. Hu, The intra-annular acylamide chelate-coordinated compound: the keto-tautomer of metal (II)–milrinone complex, J. Mol. Struct. 875 (2008) 113–120.
[36] A.K. Chandra, T.Z. Huyskens, Theoretical study of the acidity and basicity of uric acid and its interaction with water, J. Mol. Struct. Theochem. 811 (2007) 215–221.

[37] M.S. Masoud, O.H. Abd El-Hamid, Z.M. Zaki, 2-Thiouracil-based cobalt(II), nickel(II) and copper(II) complexes, Trans. Met. Chem. 19 (1994) 21–24.
[38] M.M. Moawad, Complexation and thermal studies of uric acid with some divalent and trivalent metal ions of biological interest in the solid state, J. Coord. Chem. 55 (2002) 61–78.
[39] V.V. Ramana, V.J. Thyagaraju, K.S. Sastry, Chromium complexes of uric acid – synthesis, structure, and properties, Inorg. Biochem. 48 (1992) 85–93.
[40] M.S. Masoud, A.M. Hindawy, A.A. Soayed, Structural chemistry of azo complexes, Trans. Met. Chem. 16 (1991) 372–376.
[41] R.N. Allen, P. Lipkowski, M.K. Shukla, J. Eszczynski, Vibrational analysis of complexes of urate with IA group metal cations (Li^+, Na^+ and K^+), Spectrochim. Acta 68A (2007) 639–645.
[42] R.G. Pearson, Chemical hardness and bond dissociation energies, J. Am. Chem. Soc. 110 (1988) 7684–7690.
[43] S.P. McGlynn, J.K. Smith, The electronic structure, spectra, and magnetic properties of actinyl ions: Part I. The uranyl ion, J. Mol. Spectrosc. 6 (1961) 164–187.
[44] L.H. Jones, Determination of U–O bond distance in uranyl complexes from their infrared spectra, Spectrochim. Acta 15A (1959) 409–411.
[45] G. Karagonins, O. Peter, Z. Electrochem. Ber. Bunsenges. Phys. Chem. 63 (1959) 1170.
[46] C.H. Macgillavry, G.D. Rieckin, International tables for X- ray crystallography, In: K. Lonsdale (Ed.), Physical and Chemical Tables, vol. 3, Acta Cryst., 16 (1963) 234–235.
[47] R.K. Parasher, R.C. Sharma, A. Kumar, G. Mohan, Stability studies in relation to IR data of some Schiff base complexes of transition metals and their biological and pharmacological studies, Inorg. Chim. Acta 151 (1988) 201–208.
[48] A. El-Dissouky, M.M. Abou-Sekkina, M. El-Kersh, A.Z. El-Sonbati, Metal chelates of heterocyclic Nitrogen containing ketones. XV. Five-coordinate nickel(II) and copper(II) complexes with a sulphur–nitrogen tridentate Schiff base, Trans. Met. Chem. 9 (1984) 372–375.
[49] R.G. Bhattacharyya, S.P. Mukhopadhyay, D.C. Bera, Inorg. Nucl. Chem. Lett. 16 (1980) 571–574.
[50] A.K. El-Sawaf, D.X. West, R.M. El-Bahnasawy, F.A. El-Saied, Synthesis, magnetic and spectral studies of iron(III) and cobalt(II,III) complexes of 4-formylantipyrine N(4)-substituted thiosemicarbazones, Trans. Met. Chem. 23 (1998) 227–232.
[51] E.R. Price, J.R. Wasson, Complexes with sulfur and selenium donors-X chromium(III) piperidyldithiocarbamates, J. Inorg. Nucl. Chem. 36 (1974) 67–71.
[52] A.B.P. Lever, Inorganic Electronic Spectroscopy, Elsevier Publishing Company, Amsterdam, 1968.
[53] K. Jǿrgensen, Absorption Spectra and Chemical Bonding in Complexes, Pergamon Press, 1962.
[54] B.T. Thaker, P.K. Bhattacharya, Studies in some new mixed Schiff base complexes-I, J. Inorg. Nucl. Chem. 37 (1975) 615–618.
[55] U. El-Ayaan, M.M. Youssef, S. Al-Shihry, Mn(II), Co(II), Zn(II), Fe(III) and U (VI) complexes of 2-acetylpyridine 4N-(2-pyridyl) thiosemicarbazone (HAPT); structural, spectroscopic and biological, J. Mol. Struct. 936 (2009) 213–219.
[56] S.K. Srivastava, K.B. Pandeya, H.L. Nigam, On a trinuclear copper(II)–α-mercaptopropionic acid complex, Inorg. Nucl. Chem. Lett. 11 (1975) 195–199.
[57] M.S. Masoud, M.M. El-Essawi, Electron spin resonance and mass spectra of substituted azo cresol complexes, J. Chem. Eng. Data 29 (1984) 363–367.
[58] M.S. Masoud, E.A. Khalil, A.M. Hafez, A.F. El-Husseiny, Electron spin resonance and magnetic studies on some copper(II) azobarbituric and azothiobarbituric acid complexes, Spectrochim. Acta 61A (2005) 989–993.
[59] A. Veeraray, P. Sami, N. Raman, Copper(II) complex of 3-cinnamalideneacetylacetone: synthesis and characterization, Proc. Indian Acad. Sci. (Chem. Sci.) 112 (2000) 515–521.
[60] P. Manikandan, R. Muthukumaran, K.R.J. Thomas, B. Varghese, G.V.R. Chandramouli, P.T. Manoharan, Inorg. Chem. 40 (2001) 2378–2423.
[61] Mathieu Soibinet, Isabelle Déchamps-Olivier, Aminou, X-ray crystal structure, ESR and potentiometric studies of copper(II) complexes with (2-pyridylmethyl, 3-pyridylmethyl) amine ligand, Inorg. Chem. Commun. 7 (2004) 405–409.
[62] H.A. Kuska, M.T. Rogers, R.E. Drullinger, Effect of substituents on the anisotropic electron spin resonance parameters in copper acetylacetones, J. Phys. Chem. 71 (1967) 109–114.
[63] D.R. Lorenz, J.R. Wasson, D.K. Johnson, D.A. Thorpe, J. Inorg. Nucl. Chem. 37 (1975) 2297.
[64] J. Lubczak, I. Cisek-Cicirko, B. Myśliwiec, React. Funct. Polym. 53 (2002) 113.
[65] M.S. Masoud, E.A. Khalil, E.E. El-Shereafy, S.A. Abou El-Enein, Thermal and electrical behaviour of nickel(II) and copper(II) complexes of 4-acetylamino-2-hydroxy-5-methylazobenzene, J. Thermal. Anal. 36 (1990) 1033–1338.
[66] E.S. Raper, A.M. Britton, W. Clegg, Synthesis, spectroscopy, and electrochemistry of heterocyclic thionato complexes of divalent nickel: crystal structure of tetraethylammonium fac-[tris (benzothiazoline-2-thionato) nickelate (II)], J. Chem. Soc. Dalton Trans. (1990) 3341–3345.
[67] B. Taqui Khan, K. Annapoorna, Mixed ligand complexes of ruthenium (III) EDTA with pyrimidines, Inorg. Chim. Acta 171 (1990) 157–163.
[68] N. Raman, A. Kulandaisamy, C. Thangaraja, P. Manisankar, S. Viswanathan, C. Vedhi, Synthesis, structural characterisation and electrochemical and antibacterial studies of Schiff base copper complexes, Trans. Met. Chem. 29 (2004) 129–135.
[69] E. Canpolat, M. Kaya, S. Gür, Synthesis, characterization of some Co(III) complexes with vic-dioxime ligands and their antimicrobial properties, Turk. J. Chem. 28 (2004) 235–242.
[70] N. Nishat, Rahis-ud-din, M.M. Haq, Synthesis, characterization, spectroscopic and antimicrobial activity studies of pyrimidine dithiocarbamate macrocyclic complexes, Polish J. Chem. 78 (2004) 645–652.
[71] M.N. Patel, P.A. Parmar, D.S. Gandhi, V.R. Thakkar, Antimicrobial and nuclease activity of mixed polypyridyl ruthenium(II) complexes, Inorg. Chem. Commun. 13 (2010) 1480–1484.
[72] M. Ruiz, L. Perello, R. Ortiz, A. Castineiras, C. Maichlemossmer, E. Canton, Synthesis, characterization, and crystal structure of [Cu(cinoxacinate)2] $2H_2O$ complex: a square-planar CuO_4 chromophore antibacterial studies, J. Inorg. Biochem 59 (1995) 801–810.
[73] G. Wu, G. Wang, X. Fu, L. Zhu, Synthesis, crystal structure, stacking effect and antibacterial studies of a novel quaternary copper (II) complex with quinolone, Molecules 8 (2003) 287–296.